

Discrete Scale Invariance in Topological Semimetals

Haiwen Liu,¹ Hua Jiang,² Ziqiang Wang,³ Robert Joynt,^{4,5} and X. C. Xie^{6,7,*}

¹*Center for Advanced Quantum Studies, Department of Physics,
Beijing Normal University, Beijing 100875*

²*College of Physics, Optoelectronics and Energy,
Soochow University, Suzhou 215006*

³*Department of Physics, Boston College,
Chestnut Hill, Massachusetts 02167 USA*

⁴*Kavli Institute of Theoretical Sciences,
Chinese Academy of Sciences, Beijing 100049*

⁵*Department of Physics, University of Wisconsin-Madison,
1150 Univ. Ave., Madison WI 53706 USA*

⁶*International Center for Quantum Materials,
School of Physics, Peking University, Beijing 100871*

⁷*Collaborative Innovation Center of Quantum Matter, Beijing 100871*

Abstract

The discovery of Weyl and Dirac semimetals has produced a number of dramatic physical effects, including the chiral anomaly and topological Fermi arc surface states [1–6]. We point out that a very different but no less dramatic physical effect is also to be found in these materials: discrete scale invariance. This invariance leads to bound state spectra for Coulomb impurities that repeat when the binding energy is changed by a fixed factor, reminiscent of fractal behavior. We show that this effect follows from the peculiar dispersion relation in Weyl and Dirac semimetals. It is observed when such a material is placed in very strong magnetic field B : there are oscillations in the magnetoresistivity somewhat similar to Shubnikov-de Haas oscillations but with a periodicity in $\ln B$ rather than $1/B$. These oscillations should be present in other thermodynamic and transport properties. The oscillations have now been seen in 3 topological semimetals: $ZrTe_5$, TaAs, and Bi [7–9].

*Electronic address: xcxie@pku.edu.cn

Scale invariance is a prominent ingredient in many important physical theories, perhaps most notably in the area of phase transitions. These theories contain a field $\phi(x)$ that has the property that $\phi(\lambda x) = \lambda^\Delta \phi(x)$, where λ is a continuous parameter and Δ is the scaling dimension. More rare is the occurrence of discrete scale invariance (DSI), where a similar equation holds, but only if λ takes on discrete values [10]. DSI is a characteristic of the fractal behavior that is seen in many macroscopic systems [11]. Its applicability to bound-state problems in quantum mechanics was exploited by Vitaly Efimov, who showed that it could occur in the 3-body problem in the limit of resonant scattering and who derived the energy spectrum in this case [12, 13]. These ideas have found wide application in few-body nuclear and atomic physics [10, 14]. However, DSI in bound-state problems has generally been considered only for 3- and many-body problems and it has never been experimentally observed in the solid state. In this paper we propose that DSI can occur in the 2-body problem and indeed that it has been observed in recent experiments in 3-dimensional (3D) Weyl and Dirac semimetals.

The physical systems in question are in high magnetic field and have low concentrations of mobile electrons such that the ultra quantum limit is reached, defined by the criterion that the Fermi level is in the lowest Landau level: $\ell_B \lesssim n_e^{-1/3}$ where the magnetic length $\ell_B = \sqrt{\hbar c/eB}$ and n_e is the density of charge carriers. The electrons scatter from impurities, and the temperature is sufficiently low that the electrical resistivity is entirely due to the impurity contribution. These conditions are readily achieved in modern experiments [7–9]. We shall see below from the experimental phenomenology that the impurities are of the usual types: short-range scatterers and Coulomb scatterers. We focus on the latter type - indeed it is the Coulomb potential that is the physical source of the DSI. This has dramatic consequences for the magnetoconductivity and other properties.

It is first necessary to investigate the solutions of the Coulomb problem for massless Dirac fermions. Near any Weyl point in the band structure we can write the electron Hamiltonian as

$$H\psi(\vec{r}) = \left[v \vec{\sigma} \cdot \left(\vec{p} - \frac{e\vec{A}}{c} \right) - \frac{Ze^2}{\kappa r} \right] \psi(\vec{r}) = E\psi(\vec{r}),$$

where $\psi(\vec{r})$ is a 2-component spinor. The conclusions hold also for the (only slightly more complicated) Dirac case of a 4-component spinor. Here v is the velocity, \vec{A} is the vector potential, Ze is the charge on the impurity and κ is the dielectric constant. In the actual

system the $1/r$ potential is cut off at the atomic scale r_a and the fact that it does not diverge is important [15].

When $\vec{A} = 0$ the problem is readily separated [16]. The solutions are

$$\psi_{jm}^k(\vec{r}) = f_j^k(r) y_{jm}^k(\theta, \phi) + i g_j^k(r) y_{jm}^{-k}(\theta, \phi)$$

Here the $y_{jm}^k(\theta, \phi)$ are the two-component eigenfunctions of the total angular momentum j with z -component m and the index $k = \ell$ if $j = \ell - 1/2$ and $k = -\ell - 1$ if $j = \ell + 1/2$. k effectively labels the parity. ℓ is the orbital angular momentum. We now make the substitution $F(r) = r f_j^k(r)$ and $G(r) = r g_j^k(r)$ and drop the indices for brevity. Then we find the radial equations

$$\begin{aligned} \left(E + \frac{\alpha}{r}\right) F(r) &= -\partial_r G + \frac{k}{r} G(r) \\ \left(E + \frac{\alpha}{r}\right) G(r) &= \partial_r F + \frac{k}{r} F(r) . \end{aligned} \tag{1}$$

$\alpha = Ze^2/\kappa\hbar v$ is the effective fine-structure constant. Note that we expect $\alpha \sim O(1)$ since $v \ll c$. The character of the solutions to the radial equations (1) changes abruptly at the point $\alpha = k$ [17, 18]. For $\alpha < k$ the solutions are monotonic in r and cannot show quasi-bound state behavior. This is the subcritical case. In the supercritical case $\alpha > k$, the solutions are oscillatory and quasi-bound state behavior might be expected. The corresponding problem has been solved in massive 3D systems [17, 18] and in massless systems without magnetic field [19–24]. The Klein tunneling allows the electrons to escape from the attractive potential and in fact only quasi-bound, non-normalizable states occur. The quasi-energies and widths form a geometric series. Evidence of the 2D supercritical quasi-bound states in graphene has been seen [25, 26].

Equations (1) have the property that if $F(r), G(r)$ is a solution with energy E then $F(\lambda r), G(\lambda r)$ is a solution with energy $\lambda^\Delta E$ with $\Delta = 1$ for all positive values of the continuous variable λ . The Efimov case has $\Delta = 2$. For bound and quasi-bound states, boundary conditions break the continuous invariance and give rise to DSI. In contrast to the Efimov case we deal here with a single-particle problem and no parameters in the potential need to take on special values. We also find similarities: in the supercritical regime the wavefunctions have the log-periodic form $\sin\left[\frac{1}{2}\sqrt{\alpha^2 - k^2} \ln(r) + \delta\right]$. The quasi-bound state energies and widths form a geometric series (as was also found in 2D). These are both general characteristics of DSI. The phase shift δ is set by the short-distance cutoff at r_a ,

but the details of the short-distance cutoff are otherwise unimportant. The wavefunctions are not normalizable because the solutions fall off only as r^{-1} and the normalization integral in 3D diverges at the upper limit.

The main theoretical point of this paper is that an external magnetic field B can serve as an effective cutoff at the large distance l_B . Under certain conditions to be given below this renders the states normalizable and suppresses the Klein tunneling, which converts the quasi-bound states to sharp resonances. The binding energy of these resonances depends on the field in such a way that their energy levels cross the Fermi energy at discrete values of the magnetic field that constitute a geometric series. In fact the form of the wavefunction guarantees that bound or quasi-bound states will have energies that are periodic in $\ln B$. As we will show, this leads to log-periodic behavior in B of the magneto-conductivity and other transport and thermodynamic quantities as the quasi-bound state energy levels pass through the Fermi level. This field dependence is reminiscent of the $1/B$ periodicity that characterizes Shubnikov-de Haas (SdH) and all other sorts of quantum oscillations. The SdH oscillations in 3D Dirac materials has been systematically studied recently [27]. Indeed, the log-periodic oscillations are similar in that they are a consequence of a modulation in the density of states at the Fermi energy. However, $1/B$ -periodic quantum oscillations are intrinsic to solid-state systems. The mechanism proposed here is extrinsic and could be eliminated by purging the system of Coulomb impurities.

We first present the exact solution for the quasi-energy spectrum and wavefunctions for $B = 0$ for the soft boundary condition $V(r \leq r_a) = V_0 = Ze^2/\kappa r_a$. The main results, as will be seen, do not depend on the precise form of the boundary condition. The energies and widths are the real and imaginary parts of the poles of the scattering phase shift as a function of the complex variable E . The equation is

$$\frac{g^*(s_0)}{g^*(-s_0)} = -e^{-2i\chi(-E/\hbar v)} \xi \varepsilon^{\pi s_0 \operatorname{sgn}(E)}$$

where $g(s_0) = \Gamma(1 + 2is_0) / \Gamma(1 + 2is_0 + i\alpha)$, $s_0 = \sqrt{\alpha^2 - k^2}$, and $\xi = (\alpha - \sqrt{\alpha^2 - k^2}) / k$. Γ is the usual gamma function and the definition of the function χ in terms of hypergeometric functions is given in the supplementary information. Fig.1 displays the spectrum and wavefunctions. They show the characteristic geometric series behavior $E_{n+1}/E_n = e^{-\pi s_0}$. It is instructive to compare these to the Wentzel-Kramers-Brillouin (WKB) approximation combined with the scattering method. The details are given in the supplementary infor-

maison where it is seen that the agreement of the quasiclassical approximation with the exact solution is very good. A very important consequence of DSI is that the range of validity of the quasiclassical approximation is very broad and we see that it in fact holds for all $r \gg r_a$. There is no intrinsic length scale at large distances to limit quasiclassicality.

We now apply a field $B = B\hat{z}$. The magnetic field introduces a new characteristic length ℓ_B . Effectively there is a confining potential with the characteristic length scale ℓ_B that now breaks the DSI at large $r \sim \ell_B$. The falloff of the wavefunction with r in the $B = 0$ case had the form r^{-1} - this function is normalizable in 1D. As B increases, we therefore expect the quasi-bound states to evolve into true bound states. When B is finite, then the problem is no longer exactly solvable. We consider the case that the expectation value of the Coulomb attraction is much greater than the Landau level spacing, which means that the radius r_n of the n -th quasi-bound state satisfies $r_n \ll \frac{\sqrt{2}}{2}\alpha l_B$. In this region the system still satisfies approximate spherical symmetry, and expanding in spinor spherical harmonic function reduce the problem to the radial equation, which can be numerically solved by the WKB method.

We show numerical solutions for the energy spectrum as a function of field on a *log-log* plot in Fig. 2. This is of course not a typical way to plot an energy level diagram. It is appropriate here because of the very unusual spectrum. The quasi-energies increase and the resonances sharpen as the quasi-bound states as the field increases. Only the real part of the energy spectrum is shown. The effective confining potential raises the levels ultimately into the range of higher Landau levels. The key points about the plot are that at a characteristic field for each level its energy increases very rapidly and that these characteristic fields also form a geometric series so that they are equally spaced when plotted as $\ln B^{1/2}$, as here. This is easily understood in the quasiclassical picture. The energy change occurs when $\ell_B \approx \hbar v s_0 / |E|$ and since E forms a geometric series, so do the characteristic values of B . This immediately implies that the density of electronic states at the Fermi energy is periodic in $\ln B$.

The main phenomenological point of this paper is that log-periodic oscillations have already been seen in 3 semi-metallic systems: ZrTe₅, Bi, and TaAs [7–9]. In Fig. 3a-3c we number the peaks and valleys and plot $\ln B$ vs this index at field strengths that exceed the ultra quantum limit value. This type of plot is a classic way of demonstrating $1/B$ -periodic oscillations at lower fields. We see a straight line in the 3 cases where oscillations have been

observed. This is very strong evidence for DSI in these materials. We note that the slope, which depends only on α and k varies by a factor of 2 or so from one material to another. Since α depends on the Fermi velocity and the dielectric constant, this is to be expected.

DSI has stronger consequences than simply the $\ln B$ periodicity. In fact we expect that the entire curve of a macroscopic property shows DSI, not just the peak and valley positions. To illustrate this, we compute the magneto-conductances σ_{xx} and σ_{zz} , since in experiments at high field it is generally the resistivity tensor derivable from them that are measured; other properties will be discussed at the end.

The scattering cross-section for Coulomb impurities at a fixed energy shows modulation as a function of field: as the bound state energies pass through a fixed energy the cross section will have a maximum. This effect is captured by the T-matrix approximation for the Kubo formula for σ_{xx} . We follow the classic treatment of Bastin *et al.* [28]; the details are given in the supplementary information. The formula for σ_{xx} is

$$\sigma_{xx} = \frac{4e^2}{\hbar} \ell_B^2 \left[n_s + n_C \frac{t^2}{8\pi\hbar v \ell_*^{-1} \Gamma(B)} \sum_n \frac{\Gamma^2(B)}{[E_F - E_n(B)]^2 + \Gamma^2(B)} \right], \quad (2)$$

where n_s is the density of short-range scatterers, n_C is the density of Coulomb scatters, ℓ_* the effective length along the magnetic field (which depends on microscopic details), t is the coupling strength between the bound states with the continuum of lowest Landau level states, E_F is the Fermi energy, E_n are the quasi-bound state energies as calculated and shown above, and $\Gamma(B)$ are the widths that are mainly determined by the broadening effect of overlap with the lowest Landau level. The calculations are done at zero temperature. This formula in practice is extremely well approximated by

$$\sigma_{xx} = \frac{4e^2}{\hbar} \ell_B^2 \left[n_s + n_C \frac{t^2}{8\pi\hbar v \ell_*^{-1} \Gamma(B)} \sum_n \frac{\eta^2}{\sin^2\left(\frac{s_0}{2} \ln \frac{B_n}{B_0}\right) + \eta^2} \right], \quad (3)$$

with the fitting parameters are η denoting the effective broadening factor and B_0 denoting a characteristic magnetic field. Equation (3) is an empirical formula that is convenient for fitting[10]. This formula shows explicitly that σ_{xx} peaks at log-periodic intervals. The longitudinal conductivity along the magnetic field direction can be also obtained:

$$\sigma_{zz} = \frac{e^2}{\hbar} \frac{1}{l_B^4 \cdot 16\pi^2} \left[n_s + n_C \frac{t^2}{8\pi\hbar v_F \cdot l_*^{-1} \Gamma(B)} \sum_n \frac{\Gamma^2(B)}{(E_F - E_n(B))^2 + \Gamma^2(B)} \right]^{-1}.$$

Thus, the longitudinal resistivity also satisfies the DSI property. However, we expect the DSI feature in ρ_{zz} to be harder to observe than ρ_{xx} , since the resistivity becomes smaller under large magnetic field due to the noted negative magnetoresistivity effect [29].

Equations (2) and (3) agree very well; the comparison is given as follows. Based on the relation $\sigma_{xy} = \frac{4e^2}{h} l_B^2 n_e$ (n_e denoting the total carrier density), we obtain the magnetoresistivity $\rho_{xx} \approx \sigma_{xx} \cdot \sigma_{xy}^{-2}$ (here we used the property $\sigma_{xx} \ll \sigma_{xy}$ from the experimental data [7]). In equations (2) and (3), the short-range impurity scattering term proportional to n_s gives the well-known linear-B magnetoresistivity [29]. The second term originates from the resonant scattering process with the quasi-bound states, which has not been considered previously. This new process is of course what gives rise to oscillations periodic in $\ln B$ in the magnetoconductances. This is seen in the theory and the experiments as an additional contribution to the linear in B background of ρ_{xx} . In Fig. 3d we show the comparison of the microscopic result in equation (2) and the empirical result in equation (3). The DSI feature for the resistivity oscillations become distinct in the log-log plot. The theoretic log-periodic oscillating curves is used to fit the experimental data after subtracting the non-oscillating background.

In Fig. 4 we compare our theoretical results to observations in ZrTe₅ [7], using the background subtraction method described in the supplementary information to remove the the non-oscillating background. It is very important to note that not only do the peaks and valleys show the $\ln B$ periodicity, but indeed the whole curve is log-periodic. Our calculations have been done at zero temperature, which means that at finite temperatures we need to adjust the broadening parameter η to fit experiment. We find that η^2 equals 0.34, 0.40 and 1.78 at temperatures 4.2K, 35K, and 80K, respectively. This broadening is due to the change in the Fermi function. The fits are slightly better at small fields, probably because the shift of the Fermi energy is neglected in the empirical formula. At very high fields the fit is not as good; however, this has most likely to do with the fact that at the upper limit the measurement of the field strength becomes less accurate. Importantly, the fitting parameters $B_0 = 0.27 T$ and $s_0 = 5.2$ do not change with temperature, as theory would, predict. Further investigation of the data reveals that s_0 does not appear to change from sample to sample. This is significant and since s_0 has only to do with the characteristics of the Coulomb potential, one might expect it to be rather universal within one material. The physical origin of B_0 is more complicated, since it is cutoff- and width-dependent. It does

change for different samples.

The theory may be tested in several ways.

A simple test would be to vary the density n_C of Coulomb impurities. The amplitude of the oscillations in ρ_{xx} is proportional to n_C . Varying the valence Z of the impurities would also be of great interest. The ratio of successive peaks in σ_{xx} is proportional to $\exp(-\pi s_0)$ and $s_0 = \sqrt{\alpha^2 - k^2}$ with $\alpha = Ze^2/\kappa\hbar v$. Thus the ratio should decrease as Z increases. Another possible effect of increasing Z is that more than one angular momentum channel becomes important. We have implicitly assumed above that $k = \pm 1$. Then the oscillation pattern would become more complicated. The spectrum of hydrogenic impurities in semiconductors has been tested in detail by optical experiments. This should also be possible here. Since the resonances are only sharp when the field is strong, field-dependent spectra would be needed.

Our proposal is that the impurities play the central role in creating the DSI, which means that DSI is an extrinsic effect. However, there may also exist the possibility of an intrinsic effect caused by electron-hole interactions. It may be more difficult to get into the supercritical regime since Z is fixed at $Z = 1$, but the concentrations would be higher and the collisions are particularly effective at degrading electrical current. ZrTe_5 in particular has a temperature-dependent Hall effect that seems to require both electrons and holes.

In our theory, we have neglected screening and a possible finite mass, both effects that break DSI by introducing a length scale. The simplest picture of screening is that the Coulomb interaction is cut off at the Thomas-Fermi length $L_{TF} = (4\pi e^2 \partial n / \partial \mu)^{-1/2} = 0.32\alpha^{-1/2}g^{-1/6}n^{-1/3}$, where μ is the chemical potential and g is the degeneracy including spin and number of nodes in the band structure. This means that $\ell_B < L_{TF}$ when the ultra quantum limit is reached and the $1/r$ form for the potential should be accurate for our purposes. We may also note that screening is expected to weaken as the field increases. We have also assumed zero mass for the electrons. If the mass is not zero, then there is another length $L_M = \hbar v / E_g$, where E_g is the energy gap. When these lengths are finite, then DSI holds only for states which have energies deep enough: $|E_n| > s_0 \hbar v / L_{TF}$ and $|E_n| > s_0 \hbar v / L_M$. The oscillations will only be observed when $L_M \gg \ell_B$. This condition puts constraints on the band structure.

Comparisons to experiments in 3 materials demonstrate that DSI is a common feature in topological semimetals. It is not a large effect - the amplitude of the oscillations is at most

a few per cent of the total ρ_{xx} . But it is a new form of quantum oscillation, dramatically different from SdH. As the theory shows and experiment confirms, it is only expected to occur in the ultra quantum limit of very high fields and only if the effective fine structure constant is large enough that the problem is in the supercritical regime. The physics of the log-periodic oscillations in σ_{xx} is very different from the physics of SdH oscillations. They do have one important thing in common, which is that both derive from oscillations in the density of states at the Fermi energy. As a result, nearly all thermodynamic and transport properties in metals show a $1/B$ periodicity. The same should be true of DSI but the oscillations will be periodic in $\ln B$.

-
- [1] Wan, X., Turner, A. M., Vishwanath A. & Savrasov, S. Y. Topological semimetal and Fermi-arc surface states in the electronic structure of pyrochlore iridates. *Phys. Rev. B* **83**, 205101 (2011).
 - [2] Vafeek O. & Vishwanath, A. Dirac Fermions in Solids: From High-Tc Cuprates and Graphene to Topological Insulators and Weyl Semimetals. *Annu. Rev. Condens. Matter Phys.* **5**, 83 (2014).
 - [3] Lv, B. Q., et al., Experimental discovery of Weyl semimetal TaAs. *Phys. Rev. X* **5**, 031013 (2015).
 - [4] Xu, S.-Y., et al., Observation of Fermi arc surface states in a topological metal. *Science* **347**, 294 (2015).
 - [5] Huang, X., et al., Observation of the chiral-anomaly-induced negative magnetoresistance in 3D Weyl semimetal TaAs. *Phys. Rev. X* **5**, 031023 (2015).
 - [6] Zhang, C., et al., Signatures of the Adler-Bell-Jackiw chiral anomaly in a Weyl fermion semimetal. *Nat. Commun.* **7**, 10735 (2016).
 - [7] Wang, H., et al., Discrete Scale Invariance and Fermionic Efimov States in Ultra-quantum ZrTe₅. Preprint at <https://arxiv.org/abs/1704.00995> (2017).
 - [8] Zhang, C., et al., Signature of chiral fermion instability in the Weyl semimetal TaAs above the quantum limit. *Phys. Rev. B* **94**, 205120 (2016).
 - [9] Behnia, K., Balicas, L. & Kopelevich, Y. Signatures of electron fractionalization in ultraquantum bismuth. *Science* **317**, 1729 (2007).

- [10] Braaten, E. & Hammer, H. W. Universality in few-body systems with large scattering length. *Phys. Rep.* **428**, 259 (2006).
- [11] Mandelbrot, B. *The Fractal Geometry of Nature*. (W.H. Freeman and Co., New York, 1982).
- [12] Efimov, V. Energy levels arising from resonant two-body forces in a three-body system. *Phys. Lett. B* **33**, 563 (1970).
- [13] Efimov, V. Energy levels of three resonantly-interacting particles. *Nucl. Phys. A* **210**, 157 (1973).
- [14] Hammer, H.W. & Platter, L. Efimov States in Nuclear and Particle Physics. *Annual Review of Nuclear and Particle Science* **60**, 202 (2010).
- [15] Pomeranchuk, I. & Smorodinsky, Y. On the energy levels of systems with $Z > 137$. *J. Phys. (USSR)* **9**, 97 (1945).
- [16] Schiff, L. I. *Quantum Mechanics*. (McGraw Hill, New York, 1968).
- [17] Zeldovich., Y. B. & Popov, V. S. Electronic structure of superheavy atoms. *Usp. Fiz. Nauk* **105**, 403 (1971) [*Sov. Phys. Usp.* **14**, 673 (1972)].
- [18] Greiner, W., Muller, B. & Rafelski, J. *Quantum Electrodynamics of Strong Fields*. (Springer-Verlag, Berlin, 1985).
- [19] Shytov, A.V., Katsnelson, M. I. & Levitov, L. S. Vacuum Polarization and Screening of Supercritical Impurities in Graphene. *Phys. Rev. Lett.* **99**, 236801 (2007).
- [20] Shytov, A. V., Katsnelson, M. I. & Levitov, L. S. Atomic Collapse and Quasi-Rydberg States in Graphene. *Phys. Rev. Lett.* **99**, 246802 (2007).
- [21] Pereira, V. M., Nilsson, J. & Castro Neto, A. H. Coulomb impurity problem in graphene. *Phys. Rev. Lett.* **99**, 166802(2007).
- [22] Nishida, Y. Vacuum polarization of graphene with a supercritical Coulomb impurity: Low-energy universality and discrete scale invariance. *Phys. Rev. B* **90**, 165414 (2014).
- [23] Nishida, Y. Renormalization group analysis of graphene with a supercritical Coulomb impurity. *Phys. Rev. B* **94**, 085430 (2016).
- [24] Zhang, P. & Zhai, H. Efimov Effect in the Dirac Semi-metals. Preprint at <https://arxiv.org/abs/1711.03118> (2017).
- [25] Wang, Y., et al., Observing atomic collapse resonances in artificial nuclei on graphene. *Science* **340**, 734-737 (2013).
- [26] Ovdad, O., et al., Observing a scale anomaly and a universal quantum phase transition in

- graphene. *Nat. Commun.* **8**, 507 (2017).
- [27] Wang, H.-W., Fu, B. & Shen, S.-Q. Intrinsic Magnetoresistance in Three-Dimensional Dirac Materials. Preprint at <https://arxiv.org/abs/1804.00246> (2018).
- [28] Bastin, A., Lewiner, C., Betbeder, O. & Nozières, P. Quantum oscillations of the Hall effect of a fermion gas with random impurity scattering. *J. Phys. Chem. Solids* **32**, 1811 (1971).
- [29] Abrikosov, A. A. Quantum linear magnetoresistance; solution of an old mystery. *J. Phys. A: Mathemat. Gen.* **36**, 9119 (2003).

Acknowledgements. We thank Jian Wang, Huichao Wang and Hui Zhai for helpful discussions. This work was financially supported by the National Basic Research Program of China (Grants No. 2017YFA0303301, No. 2015CB921102 and No. 2014CB920901), the National Natural Science Foundation of China under Grants No. 11674028, No. 11534001, No. 11374219, No. 11504008, and NSF of Jiangsu Province, China (Grant No. BK20160007).

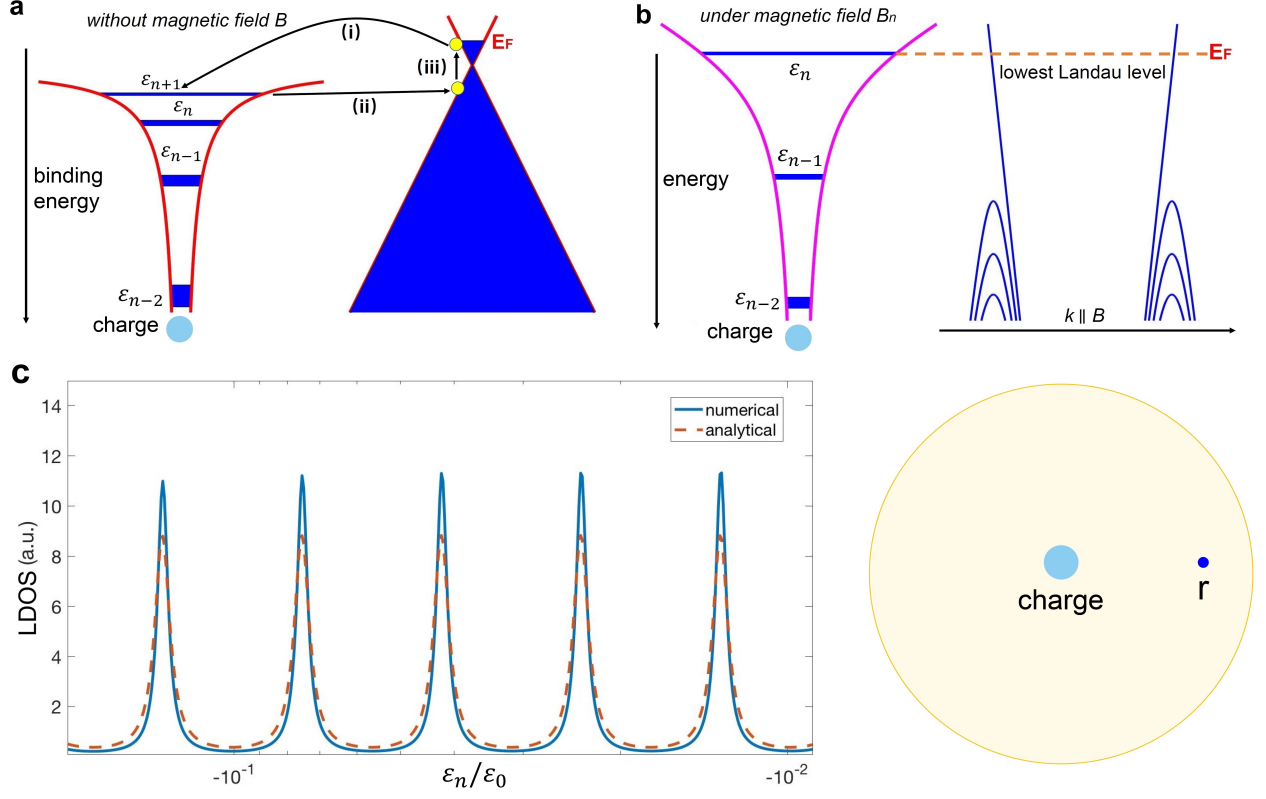


FIG. 1: The DSI properties of quasi-bound states. (a) Without magnetic field, quasi-bound states form around the charge center [process (i)]. The Klein tunneling [process (ii)] with electron-hole excitation [process (iii)] gives rise to finite widths to the quasi-bound state spectra. Due to the small Fermi surface, screening is relatively weak. (b) With a magnetic field, the potential changes in the large r region, and the quasi-bound states narrow and move to the Fermi level at certain field values B_n . The mobile carriers are in the lowest Landau level when B is in the ultra quantum limit. (c) The local density of states (LDOS) at an arbitrarily chosen location with $r \gg r_a$ as a function of the dimensionless energy showing the broad quasi-bound states. The exact analytical solutions (solid line) and the numerical WKB-type solutions (dashed line) are shown. Here $\alpha = 5.5$ and $k = 1$.

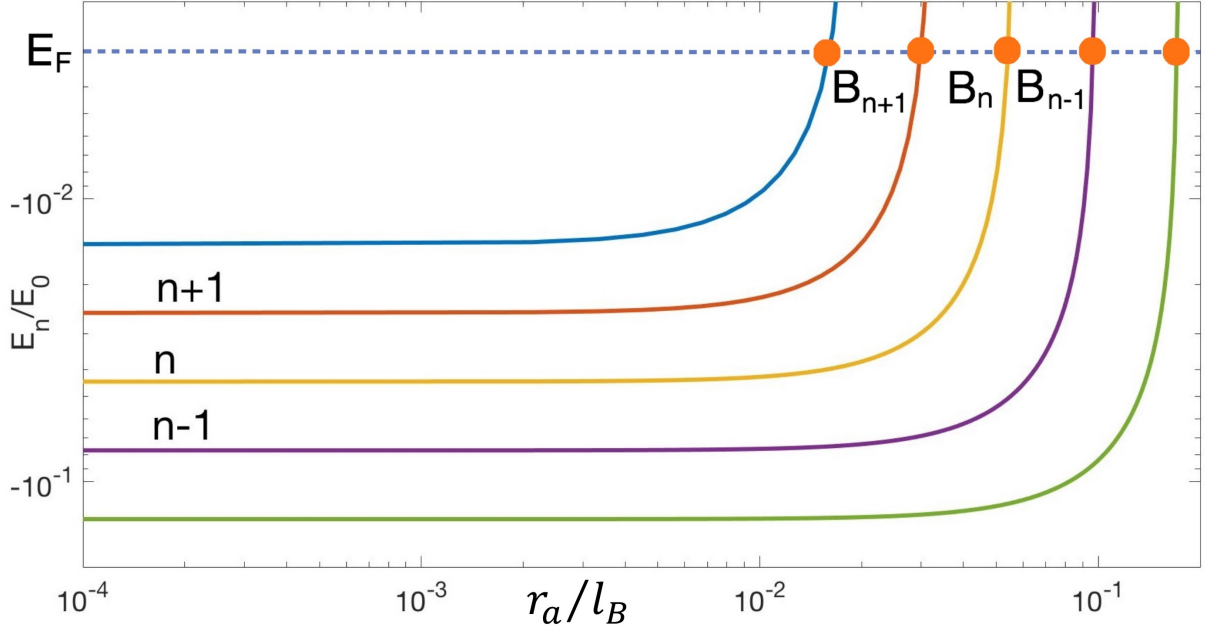


FIG. 2: The evolution of the dimensionless quasi-energy spectrum versus the dimensionless inverse magnetic length ℓ_B for the quasi-bound states. r_a is the short-range cutoff and again $\alpha = 5.5$ and $k = 1$. Only the real part of five quasi-energies are shown. The broad quasi-bound states evolve into sharp resonances in the presence of the magnetic field, and approach the Fermi energy at certain sharp values of the magnetic field strength B_n that form a geometric series.

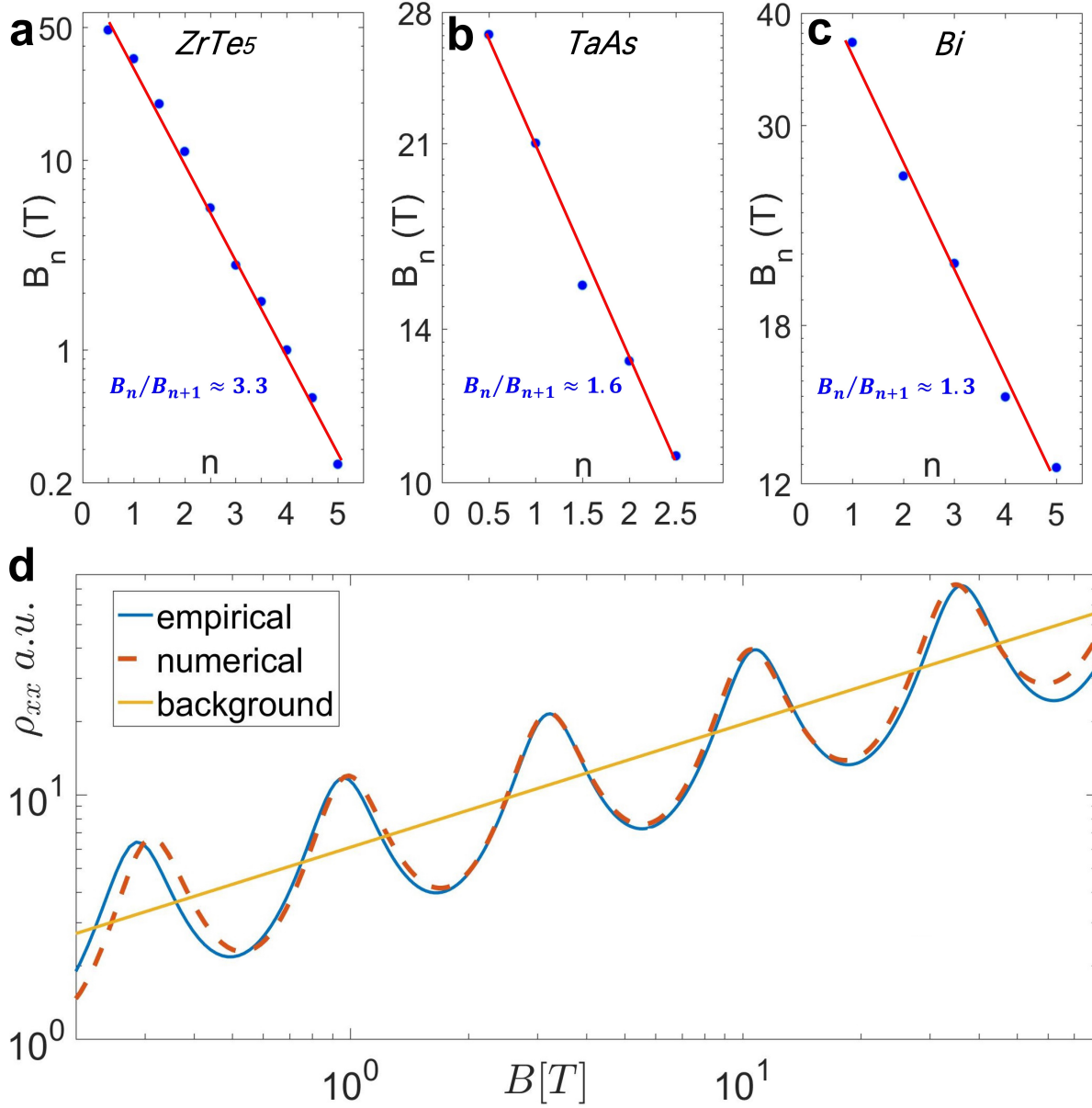


FIG. 3: The DSI features of magneto-oscillations in topological semimetals. (a)-(c) show that the peaks and dips in magneto-oscillations of $ZrTe_5$ [7], $TaAs$ [8] and Bi [9] form a geometric series. (d) A log-log plot of transverse resistivity shows oscillations satisfy the DSI property. The empirical formula (solid line), the microscopic numerical calculation (dashed line), and the non-oscillating backgrounds are also shown. Here the parameters are $\alpha = 5.3$ and $k = 1$.

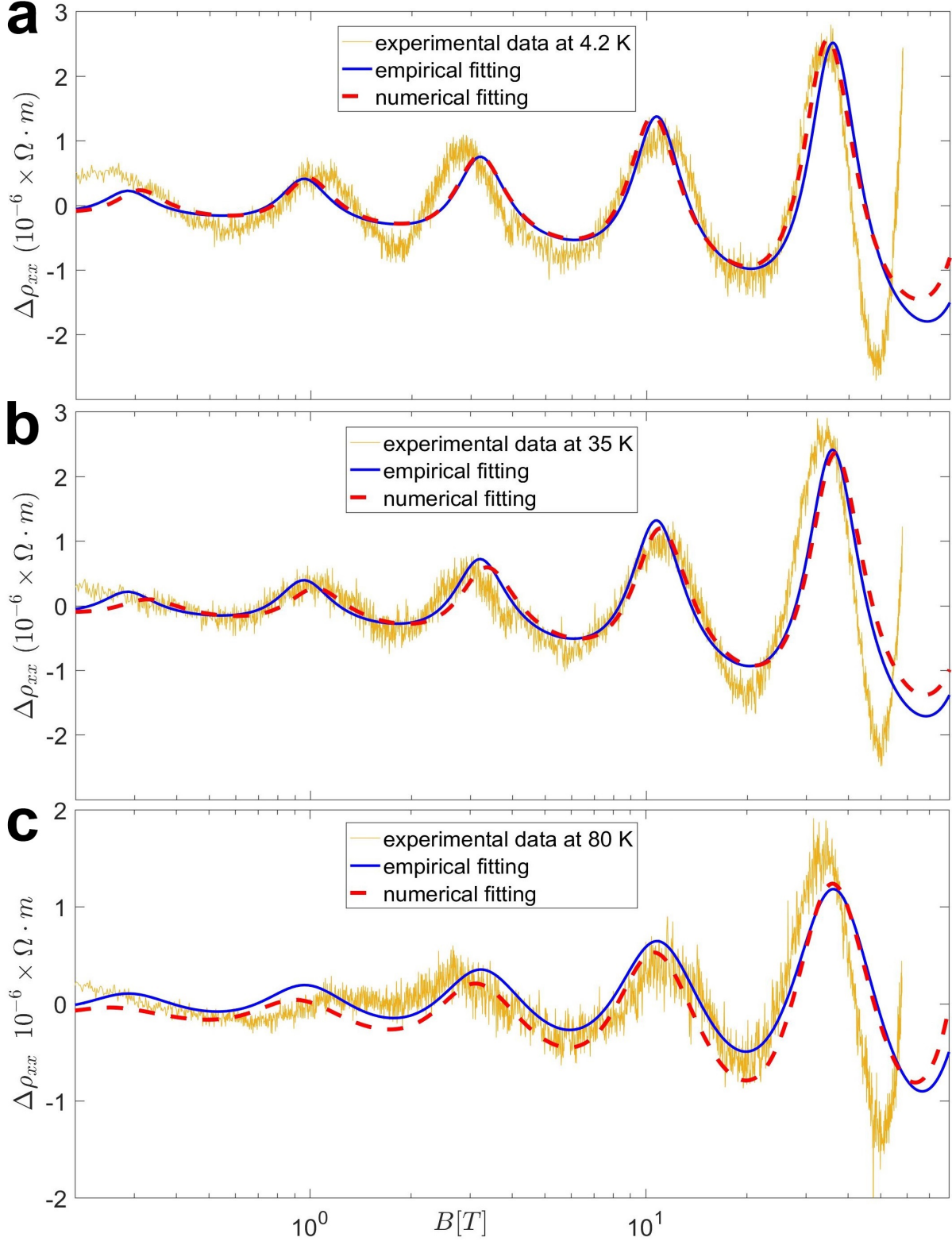


FIG. 4: The fitting of experimental data for ZrTe_5 for different temperatures. The resistance data at 4.2K (a), 35K (b) and 80K (c) are shown, with the fitting curves based on the empirical formula (solid lines) and microscopic calculations (dashed lines). The microscopic results are closer to experimental data at low field, while both empirical and numerical results fit well at high field.